Pergamon

Int. J. Heat Mass Transfer. Vol. 39, No. 18, pp. 3823–3834, 1996

0017–9310/96 $15.00+0.00

PII: S0017–9310(96)00059–2

Penetrative convection induced by the freezing of seawater

LAYACHI HADJI and XIAN-XI JIN

Department of Mathematics, The University of Alabama, Tuscaloosa, AL 35487–0350, U.S.A.

(*Received* 14 *April* 1995 *and in final form* 1 *February* 1996)

Abstract—Thermosolutal convection induced by freezing a layer of seawater from above is studied in a series of numerical experiments. The model equations take into account the dependence of the density and the temperature of maximum density on salt content, the possible presence of penetrative convection and supercooling effects. The threshold values for the onset of convection are determined over a wide range of parameter space. Two types of cell pattern are predicted by the linear theory: (1) convection of the entire fluid cell and (2) multi-layer convection. An attempt is made at quantifying the cabbeling instability associated with the onset of the latter. Only multi-layer convection prevails for supercritical Rayleigh numbers. For a specific parameter range, a flow pattern consisting of a strongly convecting layer floating between two relatively stable layers is found. The numerical experiments seem to imply that penetrative convection delays the release of heat to the atmosphere during the formation of polynyas. Copyright © 1996 Elsevier Science Ltd.

1. INTRODUCTION

In the cold regions surrounding the South Pole, a complex interplay takes place between ice, oceanic convection and the atmosphere. The ice that forms during the freezing of the antarctic water acts like an insulating barrier that inhibits the release of oceanic stored heat into the atmosphere. The major portion of this heat comes from the latent heat released during ice formation and from absorbed solar radiation. The formation of coastal or open-ocean polynyas allows for the salty water that underlies the ice to become exposed to the frigid atmosphere leading to a surge of heat into the surrounding air. The increase in the air temperature that ensues may have a significant influence on both the local and global energy balance. Indeed, amounts of heat on the order of 200 W m^{-2} are predicted to escape to the atmosphere through these openings according to the calculations of Aagaard *et al.* [1]. The reader is referred to Gordon and Comiso [2] and Smith *et al.* [3] for an extensive review of the coupled sea-ice atmosphere system in cold climates. This work is mainly aimed at achieving a better understanding of the coupled process of freezing and convection in seawater.

Before coming to the core of the subject of this paper it is useful to consider briefly the freezing of fresh water from above. This will provide insight which may help in determining the influence of salt during the freezing of seawater. Owing to the fact that fresh water solidifies at a temperature of 0°C and has a density maximum at 4°C, a stable layer, bounded by the 0 and 4°C isotherms, forms. This layer overlies a deeper layer that is generally convectively unstable and can affect the stability of the top layer through penetrative convection. This convection phenomenon was brought to light, for the first time, by Veronis [4] and was later studied by Moore and Weiss [5], Mathews [6] and Foster and Harcourt [7]. When an opening in the ice layers forms, the exchange of heat between the bottom layer and the atmosphere occurs through the top layer. Thus, the efficiency of this heat transport depends on the vigor of the convective flow in this top layer; that is to say, if the layer is nearly static, heat will mainly diffuse across it, while if it is strongly convecting, it will transport heat more efficiently. In the former case, the mode of heat transfer is slow enough that new ice will very likely form before any appreciable amount of heat escapes to the atmosphere; while in the latter case, vigorous convection occupying the fluid over all of its depth will transport heat more efficiently leading to a formation of a significant positive flux and a delay in the formation of new ice. In the work we report here, the scenario dealing with the formation of a positive heat flux in pure water is investigated for the more realistic case of seawater.

The freezing of seawater involves the coupled process of heat and salt transfer, phase transformation and natural convection. Even in the absence of freezing, the interaction between heat and salt diffusion in seawater leads to a rich variety of convective motions termed double-diffusive. Turner [8] and Schmitt [9] have reviewed the development of this important convection process. Several experimental and numerical studies dealing with the freezing of seawater have been undertaken. Foster [10] and Farhadieh and Tankin [11] have performed experiments to investigate the coupling between thermohaline convection and solidification during the freezing of seawater. The latter authors have, in particular, obtained the following data which shows the dependence of the freezing tem-

NOMENCLATURE

C	salinity
C_0	concentration at the lower plate
C_e	equilibrium freezing concentration
c	dimensionless concentration fluctuation
D	$\partial/\partial z$
D_S	coefficient of solutal diffusion [m^2 s^{-1}]
g	gravitational constant [m s^{-2}]
H	thickness of the ice layer [m]
h	depth of the stably stratified layer [m]
K_S	thermal conductivity of the solid [J m^{-1} s^{-1} K^{-1}]
K_L	thermal conductivity of the liquid [J m^{-1} s^{-1} K^{-1}]
l	depth of the unstably stratified layer [m]
M	liquidus slope [°C]
m	dimensionless liquidus slope
p	pressure [N m^{-2}]
P	Prandtl number
R_T	Rayleigh number
S	density ratio
s	growth rate
T	temperature in the mixture [°C]
T_S	temperature in the ice layer [°C]
T_0	temperature at the upper plate [°C]
T_M	temperature of maximum density [°C]
T_e	equilibrium freezing temperature [°C]
T_{int}	solid–liquid interface temperature [°C]
u	horizontal velocity [m s^{-1}]
w	vertical velocity [m s^{-1}].

Greek symbols

α_T	coefficient of thermal expansion [°C^{-2}]
σ_S	coefficient of solutal expansion
α	wavenumber
β	heat transfer coefficient at the interface
γ	penetration factor
θ	dimensionless temperature fluctuation
κ	thermal diffusivity in the mixture [m^2 s^{-1}]
κ_S	thermal diffusivity in the solid [m^2 s^{-1}]
λ	density extremum parameter
ν	kinematic viscosity [m^2 s^{-1}]
ρ_0	reference density [kg m^{-3}]
τ	Lewis number
ψ	streamfunction.

Subscripts

c	critical
L	liquid phase
s, S	solid phase.

perature, T_e, and the temperature of maximum density, T_M, on the salinity in parts per thousand (‰), (salinity, T_e, T_M): (18, −1.2, 0.2), (25, −1.5, −1.5), and (35, −2.0, −3.8). Quadratic polynominal fits for T_M and T_e are plotted in Fig. 1. We note the existence of a salinity level, $C \approx 25$‰, below which $T_M > T_e$ and above which $T_M < T_e$. Hence, in the preconvective regime, the fluid is unstably stratified over all its depth when the salt concentration exceeds 25 (‰). Brewster

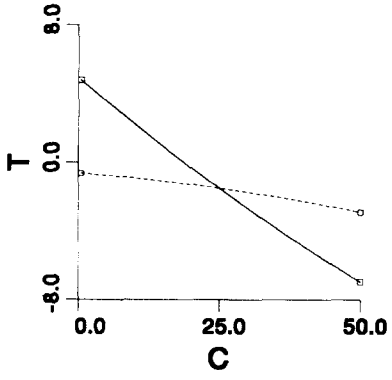

Fig. 1. Plot of the quadratic polynominal interpolations for the temperature of maximum density ($T_M = 0.000756C^2 - 0.275378C - 4.9117647$) (continuous line) and the freezing temperature ($T_e = -0.00042C^2 - 0.0247899C - 0.617647$) (dashed line).

and Gebhart [12], in their experimental study of the effects of supercooling and freezing on natural convection in seawater, have identified three fluid flow regimes in terms of a dimensionless density extremum parameter and water supercooling conditions, namely, besides the buoyancy force in the water being either upward or downward over all the liquid depth; there is also a mixed state in which it is upward in some regions of the fluid and downward in others. Further, they detect water supercooling at the cold surface before the beginning of freezing and discover that density extremum effects play an important role in heat transfer before freezing at low temperatures. Molemaker and Dijkstra [13] have performed an analysis on the stability of the boundary layer profiles of temperature and salinity that form at the moving solid–liquid interface during the freezing of seawater from above. Their numerical results show the existence of a new type of oscillatory instability in a parameter range that, according to the calculations of Baines and Gill [14], consists only of stationary instabilities. Their study makes use of realistic boundary conditions at the solid–liquid interface, but ignores the density anomaly of water. Antar [15, 16] considered convection in a mixture whose density varies quadratically with temperature and linearly with concentration, thus accounting for the density anomaly of seawater. He calculated the threshold values for the

onset of double-diffusive convection in a parameter space that included the thermal and solutal Rayleigh numbers and also the Lewis number.

In the present paper, we analyze penetrative convection in a layer of seawater underlying sea ice, with the overall aim of increasing our understanding of the influence of thermohaline convection on the positive heat flux that forms during the formation of a polynya. For this purpose, a system is considered with the geometry of the Rayleigh–Bénard type and consists of a Boussinesq dilute salt–water mixture located between two plates of infinite horizontal extent. A temperature gradient is imposed on the system in such a way that an upper portion of the mixture is frozen. A simplified model is considered in which the solid–liquid interface is assumed nonmobile and nondeformable. These assumptions are appropriate for two main reasons. The first reason is that the solid–liquid boundary movement is on a much longer time scale than the convection time scale. The second reason has to do with the fact that during the formation of the solid layer, the morphological instabilities, which are associated with the formation of the ice layer, are seemingly less important than those due to the interaction of thermohaline convection with the interface morphology. Indeed, Brewster and Gebhart [12] report important information concerning the morphology of the solid–liquid phase boundary during the downward freezing of salt water. They have observed that the dendritic interface that forms at the start of the experiment is smoothed out by the convective currents in the liquid, thereby giving way to an almost planar interface at the end of the experiment. These observations seem to support our assumption of negligible deformation. In this case, the solidified layer plays the role of an upper boundary whose thermal conductivity is comparable to that of the liquid mixture and in which heat transfer occurs by conduction alone. Solute diffusion in the solid phase is considered slow enough that it can be ignored. The temperature of the solid–liquid interface, which is obtained from the idealized phase diagram, depends linearly on concentration with slope $M < 0$, where M is the liquidus slope.

The content and organization of this paper are outlined in the following way. In Section 2, we formulate the mathematical description of the system, solve for the basic state and derive the governing system for the fluctuations. The linear stability analysis is presented in Section 3 and the nonlinear results of the numerical simulations are described in Section 4. Finally, some concluding remarks are given in Section 5.

2. FORMULATION

We consider a horizontally unbounded layer of seawater of depth d, confined between two rigid isothermal plates. See Fig. 2 for a schematic diagram. A temperature gradient is imposed on the system in such a way that an upper portion of the mixture is frozen. The temperature in the ice layer T_S satisfies the heat conduction equation

$$\frac{\partial T_S}{\partial t} = \kappa_S \nabla^2 T_S. \tag{1a}$$

In the liquid phase, the system evolution is described by the following conservation equations for momentum, heat, solute and mass, respectively:

$$\frac{\partial u}{\partial t} + u\frac{\partial u}{\partial x} + w\frac{\partial u}{\partial z} = -\frac{1}{\rho_0}\frac{\partial p}{\partial x} + \nu\nabla^2 u \tag{1b}$$

$$\frac{\partial w}{\partial t} + u\frac{\partial w}{\partial x} + w\frac{\partial w}{\partial z} = -\frac{1}{\rho_0}\frac{\partial p}{\partial z} + \nu\nabla^2 w + \frac{\delta\rho}{\rho_0}g \tag{1c}$$

$$\frac{\partial T}{\partial t} + u\frac{\partial T}{\partial x} + w\frac{\partial T}{\partial z} = \kappa\nabla^2 T \tag{1d}$$

$$\frac{\partial C}{\partial t} + u\frac{\partial C}{\partial x} + w\frac{\partial C}{\partial z} = D_S\nabla^2 C \tag{1e}$$

$$\frac{\partial u}{\partial x} + \frac{\partial w}{\partial z} = 0, \tag{1f}$$

where u and w are the horizontal and vertical components of the velocity vector field, T is the temperature in the liquid phase, C is the concentration, p is the pressure, ρ_0 is a reference density, ν is the dynamic viscosity, and κ and κ_S are the thermal diffusion coefficients in the liquid and solid phases, respectively; $\delta\rho$ represents the density change that is induced by temperature and concentration variations and is described by the following equation of state:

$$\delta\rho = \rho_0[1 - \alpha_T(T - T_M)^2 + \alpha_S(C - C_M)], \tag{2}$$

where C_M is the concentration at T_M, α_T and α_S are the thermal and solutal expansion coefficients, respectively, and D_S is the coefficient of solutal diffusion.

Next we introduce the boundary conditions that supplement equations (1a–f). Continuity of temperature and of the heat flux at the solid–liquid interface located at $z = d$ yields

$$T = T_S = T_{int} \quad K_S\frac{\partial T_S}{\partial z} = K_L\frac{\partial T}{\partial z}. \tag{3a}$$

Here K_S and K_L are the thermal conductivities in the solid and liquid phases, respectively, and T_{int} is the freezing temperature of seawater which depends on salt content as follows:

$$T_{int} = MC \quad M = \frac{dT_{int}}{dC}(C = 0). \tag{3b}$$

The effects due to the rejection of salt upon freezing are included in the model through the coupled boundary condition, equation (3b). The boundary conditions at the plates located at $z = 0$ and $z = d + H$, H being the thickness of the ice layer, are (cf. Fig. 2)

$$T = T_B \quad u = w = 0 \quad T_S = T_0 \quad C = C_0. \tag{3c}$$

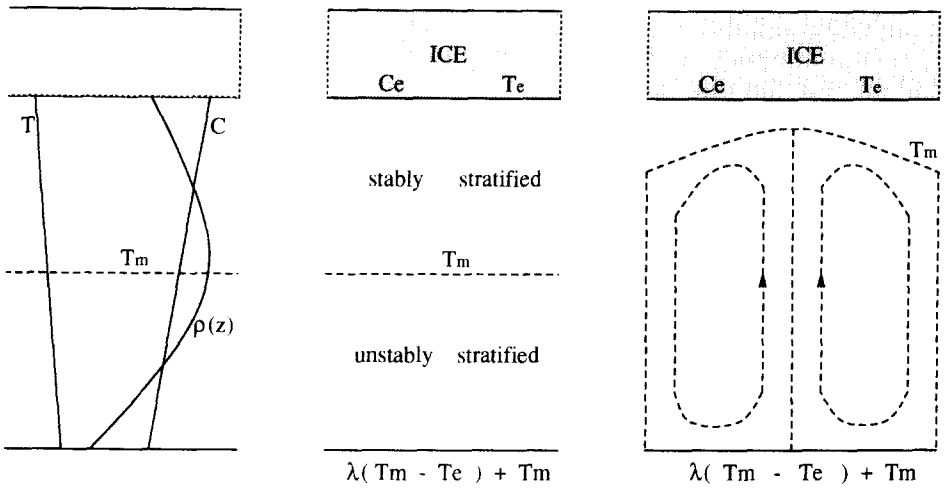

Fig. 2. Sketch of a layer of seawater underlying a layer of sea-ice of thickness H. The dotted line represents the maximum density isotherm which is horizontal in the preconvective regime (middle) and distorted as it conforms to the convection pattern (right). The conduction profiles of temperature and concentration and associated density profile are shown on the left.

In the absence of convection, the basic profiles of temperature and concentration are linear in the vertical variable, and are given by

$$\mathscr{T}(z) = T_M - (h-z)\frac{T_M - T_B}{h} \tag{4a}$$

$$\mathscr{C}(z) = C_M - (h-z)\frac{(C_c - C_B)}{d}. \tag{4b}$$

If we let l denote the height of the stably stratified layer, and h the height of the unstably stratified layer ($d = l+h$), then the evaluation of the temperature at the ice–water interface, located at $z = l+h$, yields

$$\mathscr{T}(l+h) = T_c = T_M + l\frac{(T_M - T_B)}{h}. \tag{5}$$

from which we deduce that

$$\frac{h}{l} = \frac{T_B - T_M}{T_M - T_c} \equiv \lambda. \tag{6}$$

Equation (6) expresses the equality of the heat flux in the stably stratified and unstably stratified layers. The parameter λ is introduced to control the temperature of the lower boundary. It also serves to regulate the initial location of the isotherm corresponding to maximum density, i.e. in the preconvective regime, the location of the T_M isotherm can be moved upward by increasing the value of the parameter λ. As $\lambda \to 0$, $T_B \to T_M$, so that the T_M isotherm approaches the lower plate resulting in a stable stratification throughout the liquid layer; and as $\lambda \to \infty$, $T_c \to T_M$ and the isotherm of maximum density coincides with the solid–liquid interface leading to a situation in which the liquid is unstably stratified over all of its depth.

The system is made dimensionless by scaling the length by the depth h of the layer that is bounded by the lower plate and the T_m isotherm, time by h^2/κ, velocity of κ/h, temperature by the difference $(T_B - T_M)$, and concentration by $(C_B - C_c)$. Upon subtraction of these mean quantities from the total quantities in equations (1a–f), we obtain the following governing system for convective fluctuations:

$$\frac{\partial \theta_s}{\partial t} = \nabla^2 \theta_s \tag{7a}$$

$$\frac{\partial \theta}{\partial t} - \frac{\partial \psi}{\partial x} - \frac{\partial \psi}{\partial z}\frac{\partial \theta}{\partial x} + \frac{\partial \psi}{\partial x}\frac{\partial \theta}{\partial z} = \nabla^2 \theta \tag{7b}$$

$$\frac{\partial c}{\partial t} - \frac{\partial \psi}{\partial x} - \frac{\partial \psi}{\partial z}\frac{\partial c}{\partial x} + \frac{\partial \psi}{\partial x}\frac{\partial c}{\partial z} = \tau \nabla^2 c \tag{7c}$$

$$\nabla^4 \psi = 2R_T(z-1)\frac{\partial \theta}{\partial x} + R_T S\frac{\partial c}{\partial x} - 2R_T\theta\frac{\partial \theta}{\partial x}, \tag{7d}$$

where θ and c are the temperature and concentration fluctuations in the liquid, respectively; θ_s is the temperature deviation in the solid phase and ψ is the stream function defined by

$$u = -\frac{\partial \psi}{\partial z} \quad w = \frac{\partial \psi}{\partial x}. \tag{7e}$$

The dimensionless parameters which appear in equations (7) are: the Lewis number τ ($\approx 1/80$ for seawater), the thermal Rayleigh number R_T, the density ratio S and the dimensionless liquidus slope m. These are defined as follows:

$$\tau = \frac{D_S}{\kappa} \quad R_T = \frac{\alpha_T g h^3 \Delta T^2}{\nu\kappa} \quad S = \frac{\alpha_S \Delta C}{\alpha_T \Delta T^2} \quad m = M\frac{\Delta C}{\Delta T}, \tag{8}$$

where $\Delta T\,(>0)$ and $\Delta C\,(<0)$ are the temperature and concentration differences between the plate and the ice–seawater interface, respectively. Our model pertains to a situation in which the density ratio S is

negative. This is due to the fact that the rejection of salt during the freezing process raises the salinity of the water layer that is in the vicinity of the sea-ice. We have accounted for the sign of the density ratio S once and for all in equation (7d). The calculations are, henceforth, performed as functions of the magnitude of S only. In deriving the set of equations (7a–d), we have ignored the inertial effects and kept the convective nonlinear terms, since the purpose of this analysis is to understand the thermal and solutal effects rather than the hydrodynamic effects, thus the Prandtl number ($P \approx 7$ for seawater) is not a relevant parameter in this analysis. Further, we have neglected any changes in the physical properties of seawater upon freezing.

The boundary conditions associated with equations (7) are as follows:

$$\theta_s = 0 \quad \text{on } z = 1 + 1/\lambda + H/h \tag{9a}$$

$$\theta = \theta_s \quad \frac{\partial \theta}{\partial z} = \frac{\partial \theta_s}{\partial z} \quad \text{on } z = 1 + 1/\lambda \tag{9b}$$

$$c = \frac{\theta}{m} \quad \text{on } z = 1 + 1/\lambda \tag{9c}$$

$$\theta = c = 0 \quad \text{on } z = 0 \tag{9d}$$

$$\psi = D\psi = 0 \quad \text{on } z = 0 \quad \text{and } z = 1 + 1/\lambda. \tag{9e}$$

The governing system can be further simplified as follows: the steady form of the heat conduction equation in the solid phase, equation (7a), is eliminated and its effect incorporated into a set of reformulated boundary conditions for the temperature in the liquid phase at the solid–liquid interface. Using normal modes in the x variable, the solution to the steady form of equation (7a) is given by

$$\theta_s(x, z) = B \sinh\left[z - (1 + 1/\lambda + H/h)\right] \exp(\iota \alpha x) \tag{10}$$

The two boundary conditions for θ, equations (9b), imply

$$\theta(x, 1 + 1/\lambda) = -B \sinh(H/h) \exp(\iota \alpha x)$$

$$\text{and} \quad \frac{\partial \theta}{\partial z}(x, 1 + 1/\lambda) = B \cosh(H/h) \exp(\iota \alpha x), \tag{11}$$

where B is an integration constant. The elimination of the constant B from equations (11) leads to the following radiation boundary for θ:

$$\frac{\partial \theta}{\partial z} = -\coth(H/h)\theta \equiv -\beta\theta \quad \text{on } z = 1 + 1/\lambda, \tag{12}$$

where $\beta = O(1)$ is a heat transfer coefficient.

In the next sections, we will present the results of the linear stability analysis and of the nonlinear numerical experiments. The neutral stability curves, the flow patterns and the distributions of temperature and salt concentrations depend on five dimensionless parameters: λ, which is the ratio of the depth of the unstably stratified layer to that of the stably stratified layer in the preconvective regime, the Rayleigh number R_T, the density ratio S ($S > 0$); the liquidus slope m and β which is the solid–liquid interface heat transfer coefficient. Results are shown for one pair of values for β and m, namely, $\beta = 1$ and $m = 1$. The influence of the variation of m on the flow pattern is discussed in Section 4.

3. LINEAR STABILITY RESULTS

We neglect the nonlinear terms in the governing system, which now consists of equations (7b–d) and boundary conditions, equations (9c–e) and equation (12). For the horizontally unbounded fluid layer, we consider Fourier modes of the form

$$\left[\theta, c, \frac{\partial \psi}{\partial x}\right] = [F(z), G(z), H(z)] \exp(\iota \alpha x) \exp(st), \tag{13}$$

where α is the real horizontal wavenumber and $s = \sigma + \iota\omega$ is the growth rate. For the case at hand, the linear stability analysis will be performed with the assumption of exchange of stabilities, i.e. the bifurcation from the motionless basic state is stationary, and the marginally stable state corresponds to $\sigma = \omega = 0$. This assumption is validated by the following argument. Initially, seawater that is right beneath the ice is both colder and saltier than the deeper water, and consequently both the heat and the sat gradients are destabilizing. Therefore, the gradients of both diffusing quantities of salt and heat collaborate to amplify any small perturbation in the liquid, thus initiating a stationary convective motion. The resulting eigenvalue problem takes the form

$$(D^2 - \alpha^2)F(z) + H(z) = 0 \tag{14a}$$

$$\tau(D^2 - \alpha^2)G(z) + H(z) = 0 \tag{14b}$$

$$(D^2 - \alpha^2)^2 H(z) + \alpha^2 R_T(z - 1)F(z) + \alpha^2 R_T S G(z) = 0, \tag{14c}$$

with corresponding boundary conditions

$$G = F = H = DH = 0, \quad \text{on } z = 0, \tag{15a}$$

$$DF = -\beta F, G = F/m, H = DH = 0, \quad \text{on } z = 1 + 1/\lambda. \tag{15b}$$

The eigenvalue problem, which now consists of equations (14a–c) and corresponding boundary conditions, equations (15a, b), is solved by the shooting method [17]. Four linearly independent starting vectors, each satisfying the boundary conditions at $z = 1 + 1/\lambda$, are chosen. The integration is then performed using a Runge–Kutta scheme with adaptive stepsize control, thus obtaining a set of eight linearly independent solutions. The required solutions of the

eigenvalue problem can be written as a superposition of these solutions. Upon application of the matching boundary conditions at $z = 0$, a system of eight linear and homogeneous equations for the coefficients is obtained. The solvability requirement of this system of equations is the vanishing of an 8×8 determinant. The numerical task of determining the zeros of the determinant is accomplished by using a bisection method that is based on Brent's algorithm [18]. The root that is of concern to us is the value of the Rayleigh number, R_T, as a function of the wavenumber α. The minimum of R_T and the corresponding value of α are the critical Rayleigh number, R_{Tc}, and the critical wavenumber, α_c, for the onset of convection, respectively. The knowledge of these threshold values, and their dependence on the remaining pertinent parameters, is required in order to understand the instability mechanisms of the top layer. The values of the critical Rayleigh numbers and corresponding wavenumbers determined in this fashion as a function of the density ratio S and of the density extremum parameter λ are given in Tables 1 and 2. The destabilizing effect of the parameter S is apparent from these results. The increase of the critical Rayleigh number with λ has to do with the fact that the depth of the convection layer increases with λ. The wavenumbers characterizing the marginal states show sharp decrease with increasing S values and a slow increase with λ. The computed wavenumbers are not, however, very accurate due to the fact that the unimodal marginal curves are flat near their minimum.

The influence of salt content and density extremum effects on the eigenfunctions of the linear problem, is shown in Fig. 3. The flow pattern portrayed by the velocity profiles in Figs (3a–c), show that for $S = 0$ and $\lambda < 1$ there is a main cell near the hot plate and weak counter-rotating cells near the cold plate. Whenever λ exceeds the value 1 or $S > 0.001$, the induced vortices disappear leaving the way to one positive cell occupying all the fluid layer. We also note that the number of induced vortices increases as λ decreases below 1. The temperature and concentration distributions also show a sign change for $\lambda = 0.4$ or smaller, and no sign change for $\lambda > 0.6$. In the preconvective state, the interface which corresponds to the location of the isotherm of maximum density is located at $z = 1$ in nondimensional units. At the onset of convection and depending on the parameters λ and S, convection takes place either as one cell over the entire liquid layer or as multi-layer convection. In the former case, which corresponds to the parameter range $S > 0.001$, the interface has moved up all the way to the upper boundary which coincides with the sea–ice–liquid interface. The presence of salt, therefore, inhibits the formation of multi-layer convection. The latter case, which corresponds to $S = 0$ and $\lambda < 1$, is analogous to the case of pure water. We have also estimated from the plots of the eigenfunctions of the linearized problem the amount by which the isotherm of maximum density in the conduction state has moved upward as a result of convection. Thus, following Moore and Weiss [5], we define the penetration factor, γ, as the ratio of the depth of the main cell to the total depth of the fluid layer. The amount of penetration as a function of λ and S is displayed in Tables 3(a) and (b). We find that γ increases with λ and S and reaches asymptotically the value 1 whenever $\lambda \geqslant 1$ or $S > 0.01$. Note that these results are valid only at the onset of convection. For more vigorous flows the nonlinearities in the governing equations must be included. This is done in the next section.

4. NONLINEAR RESULTS

We have undertaken a numerical nonlinear analysis of the governing equations, equations (7a–d), and corresponding boundary conditions, equations (9c,d) and equation (12), in a cavity of width equal to one-half of one wavelength as determined from the linear stability analysis and height $(1 + 1/\lambda)$. The boundary conditions are supplemented by conditions at the horizontal wall of the half cell,

$$\psi = \frac{\partial \psi}{\partial x} = \frac{\partial \theta}{\partial x} = \frac{\partial c}{\partial x} = 0 \quad \text{on } x = 0 \quad \text{and } x = \frac{\pi}{\alpha_c}. \tag{16}$$

Table 1. The critical Rayleigh number R_c as a function of the parameter λ and the density ratio S

	$S = 0.0$	0.00005	0.00025	0.0005	0.005	0.025	0.05
$\lambda = 0.65$	517	517	517	513	240	30	12
1.0	595	590	570	548	279	42	28
2.0	602	600	575	560	355	132	74

Table 2. The critical wavenumber α_c as a function of the parameter λ and the density ratio S

	$S = 0.0$	0.00005	0.00025	0.0005	0.005	0.025	0.05
$\lambda = 0.65$	2.06	2.06	1.97	1.97	1.65	1.29	1.25
1.0	2.10	2.06	2.06	1.90	1.70	1.60	1.53
2.0	1.94	1.96	1.97	2.03	2.03	2.03	2.03

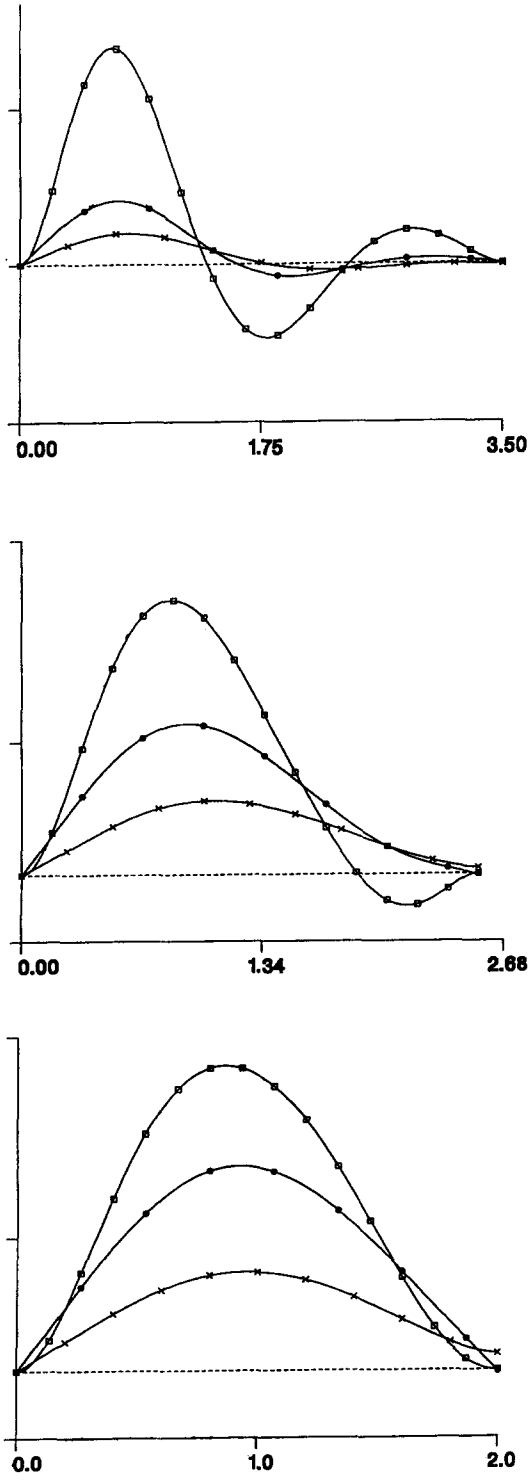

Fig. 3. Plots of the eigenfunctions ψ, (□), temperature θ, (×) and concentration c, (●) for: $S = 0$ and $\lambda = 0.4$ (top), $S = 0$ and $\lambda = 0.65$ (center), $S = 10^{-3}$ and $\lambda = 1.0$ (bottom). Other parameters are $\tau = 0.0125$, $\beta = 1$ and $m = 1$.

The dimensionless conservation equations are solved numerically utilizing the finite difference method. We proceed by first solving the momentum equation (7d) for ψ. The three terms that appear on the right hand side of equation (7d) are used as source terms [19]. The equation is descretized by making use of second-order accurate central difference representation for the spatial derivatives and the resulting system solved by utilizing the successive over-relaxation (SOR) iterative method. The iterations are terminated when the values of the streamfunction agree to six significant digits at each grid point. These results are then utilized in the heat and concentration equations, equations (7b, c), and a similar routine is used for θ and c. Finally, a converged solution is achieved when all the dependent variables are such that the difference between two successive iterations are simultaneously less than 10^{-6}. The nonlinear calculations are perfomed on a Cray-C90 computer and require up to 4 h of CPU time for one simulation corresponding to a set of values of the parameters. We have noticed an increase in computation time with increases in either the Rayleigh number or the density ratio and we failed to obtain a converged solution for relatively large R_T or S.

Table 3.

(a) Variation of the penetration factor γ with the density ratio S for $\lambda = 0.65$

S:	0.0	0.0001	0.001	0.01
γ:	0.712	0.744	0.783	1

(b) Variation of the penetration factor γ with the parameter λ for $S = 0$

λ:	0.4	0.5	0.65	1.0
γ:	0.394	0.469	0.712	1

4.1. *The case* $\lambda > 1$

Figure 4 (top part) depicts streamlines for $\lambda = 2$, $S = 0$ and three values of the Rayleigh number. For this specific range of parameters, convection takes place in the form of one large cell occupying the whole fluid layer at $R = 602$. As R increases from its critical value, we note the appearance of a pair of counter-rotating corner vortices at the warm plate. As these vortices gain in intensity, they occupy a larger portion of the fluid layer by squeezing the large positive cell and a progressive narrowing of the bottom of the main cell ensues. This is accompanied by a noticeable downward movement of the center of the positive cell and the appearance of another negative cell in the vicinity of the solid–liquid interface. The fluid layer divides into two separate regions: a strong convective flow in the lower part of the layer and a weak flow adjacent to the solid–liquid interface.

The influence of the density ratio S on the flow patterns is shown in the lower part of Fig. 4. It is seen that, except for the fact that the flows are less rigorous, the flow patterns have the same overall qualitative features as in the case $S = 0$ shown in Fig. 4(a). It is also noteworthy to add that, even for the case $S = 0$ which corresponds to a vanishing coefficient of solutal expansion, the convective fluctuations for the salt con-

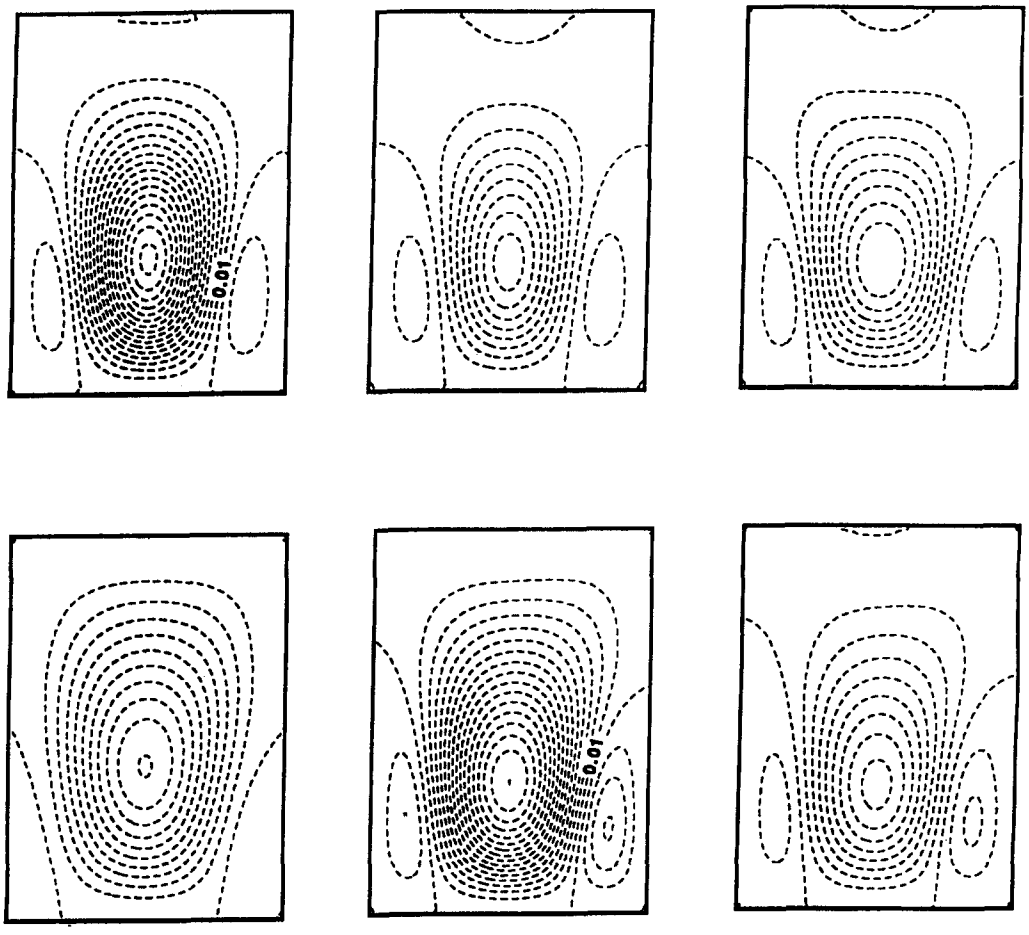

Fig. 4. Streamfunction contours for $\lambda = 2.0$ and Rayleigh numbers (from left to right) $R = 1000$, 1500 and 2500; $S = 0$ (top) and $S = 0.05$ (bottom). Other parameters are $\tau = 0.0125$, $\beta = 1$ and $m = 1$.

centration still arise as a result of the coupling between the temperature and concentration fields at the solid–liquid interface [equation (9c)]. Consequently, the results pertaining to the single-component liquid case cannot be retrieved from our analysis and only a qualitative comparison with the nonlinear results of Moore and Weiss [5] is possible.

The influence of the Rayleigh number and the density ratio on the steady-state distributions of temperature and concentration are illustrated in Fig. 5. We consider two pairs of values for R_T and S. The first pair is $R_T = 100$ and $S = 30$ and the second is $R_T = 1100$ and $S = 0.6$ (about 30 R_c). In both cases, we notice a definite tendency toward the formation of concentration boundary layers near the solid–liquid interface, the lower plate and also at the boundary between the main cell and the induced vortices, and an almost isohaline core in the rest of the fluid region. The equilibrium temperature distribution is, however, only weakly distorted (the isotherms are mainly horizontal throughout the fluid layer).

4.2. *The case* $\lambda < 1$

The plots of streamlines that are shown in Fig. 6(a) correspond to $\lambda = 0.65$ and $S = 0$. We follow the evolution of the cell pattern with increasing R_T in a box of size 1.52×2.65 with R_T ranging from 1800 to 4000 (i.e. up to 8 R_c). When $R_T = 1800$, there is one large positive cell that is elongated in the vertical direction and whose center lies close to the bottom plate (the center of the cell being a point of maximum velocity). As the Rayleigh number is increased, the cell becomes less elongated and at $R \approx 3000$ a counter-rotating cell appears in the upper part of the fluid layer. Furthermore, intense motion is observed near the lower plate and no noticeable movement of the center of the cell is detected.

The influence of the solutal effects on the cell pattern is depicted in Fig. 6(b). This pattern corresponds to $\lambda = 0.65$ $R_T = 100$ and S ranging from 0.5 to 30. Initially, only one elongated positive cell occupies all the box. At $S \approx 2$, two counter-rotating vortices appear in the upper left and lower right corners. The main positive cell becomes skewed to the right under the squeezing action of these vortices. As S is further increased, the convection flows that initiate in the corner vortices penetrate the neighboring positive cell, thus leading to a cell pattern that consists of a flat positive cell that is sandwiched between two negative cells. These negative cells are regions of weak convec-

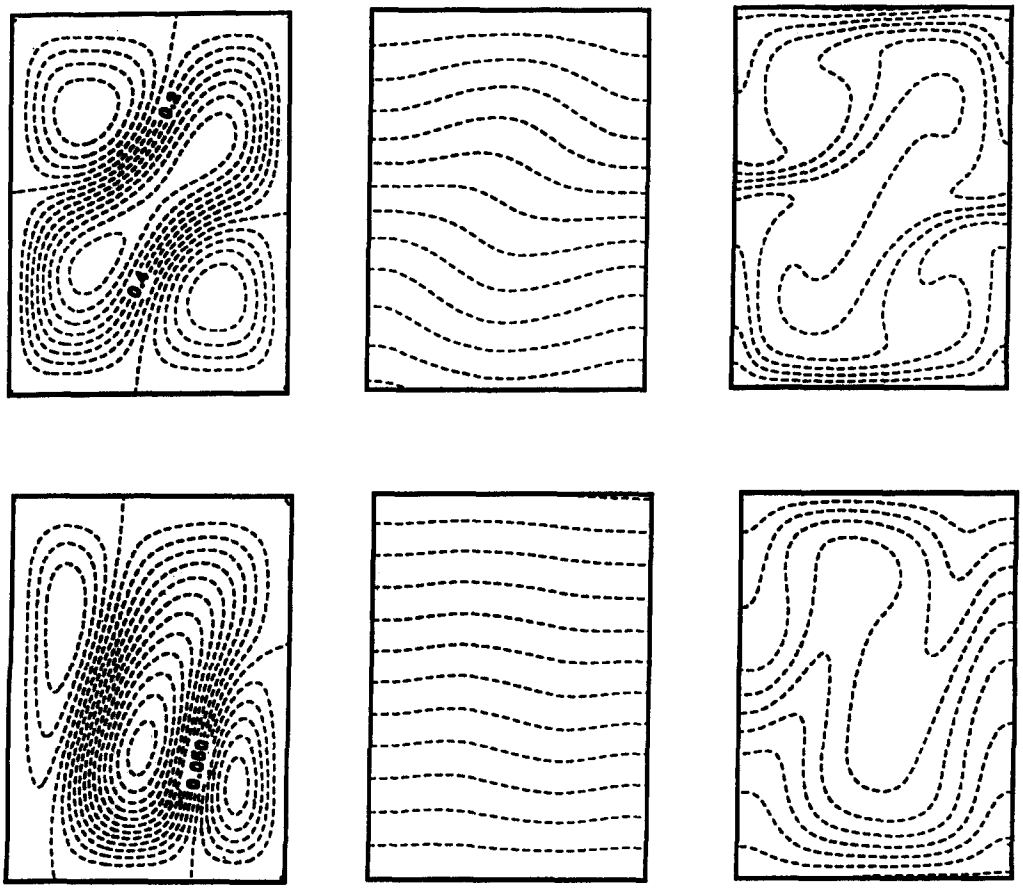

Fig. 5. Streamfunction contours, isotherms and contours of equal concentration for $\lambda = 2$ and $S = 30$ $R_T = 100$ (top) and $S = 0.6$, $R_T = 1100$ (bottom). Other parameters are $\tau = 0.0125$, $\beta = 1$ and $m = 1$.

tion. This symmetric configuration resembles the cell pattern associated with an S-shaped, cubic temperature profile, and a density that varies linearly with temperature [6]. We postulate that further increases in S will lead to the formation of floating convection: a strongly convecting layer located in the middle of the fluid cell and bounded below and above by two relatively stable layers.

The corresponding temperature and concentration distributions are shown in Fig. 7 for $S = 30$ and $R_T = 100$. We observe the appearance of concentration boundary layers at the lower plate, the solid–liquid interface and at the boundaries between the vortices. The centers of these vortices form large cores that are both isothermic and isohaline.

Figure 8 shows lines of equal concentration for $R_T = 500$, $S = 0$, $\lambda = 2$ and three values of m. As the magnitude of m is increased, which corresponds to an increase in supercooling at the phase boundary, sharp changes in salt concentration are seen to develop near the solid–liquid interface. Here the supercooling is defined as the difference between the actual water temperature and its freezing temperature, i.e. $(T-mC)$, so that increases in m lead to an increase in supercooling. The equal concentration contours remain primarily unchanged away from the solid–liquid interface, and the streamlines and isotherms are unaffected by changes in m. This figure, which corresponds to only one set of parameters, does depict all possible behavior. Other values of λ or S yield similar outcomes.

5. CONCLUDING REMARKS

We have analyzed in some detail the influence of freezing on penetrative convection in a layer of seawater by adopting a Bénard-like set-up, in which a layer of a dilute salt-water mixture is partially solidified from above. The main goal of this paper is to extend previous studies on penetrative convection in pure water [4, 5] to the case of seawater. This extension has been revealed to be a delicate one, due to the coupling between the concentration and temperature fields. This arises for two reasons; firstly, the freezing temperature of seawater depends on the salt concentration [equations (3)]. This dependence is obtained from an idealized phase diagram. Secondly, unlike pure water whose density is maximum near 4°C, the temperature of maximum density of seawater also depends on salt content. Casting the model in dimensionless form has helped to isolate the relevant control parameters. Besides the usual thermal Ray-

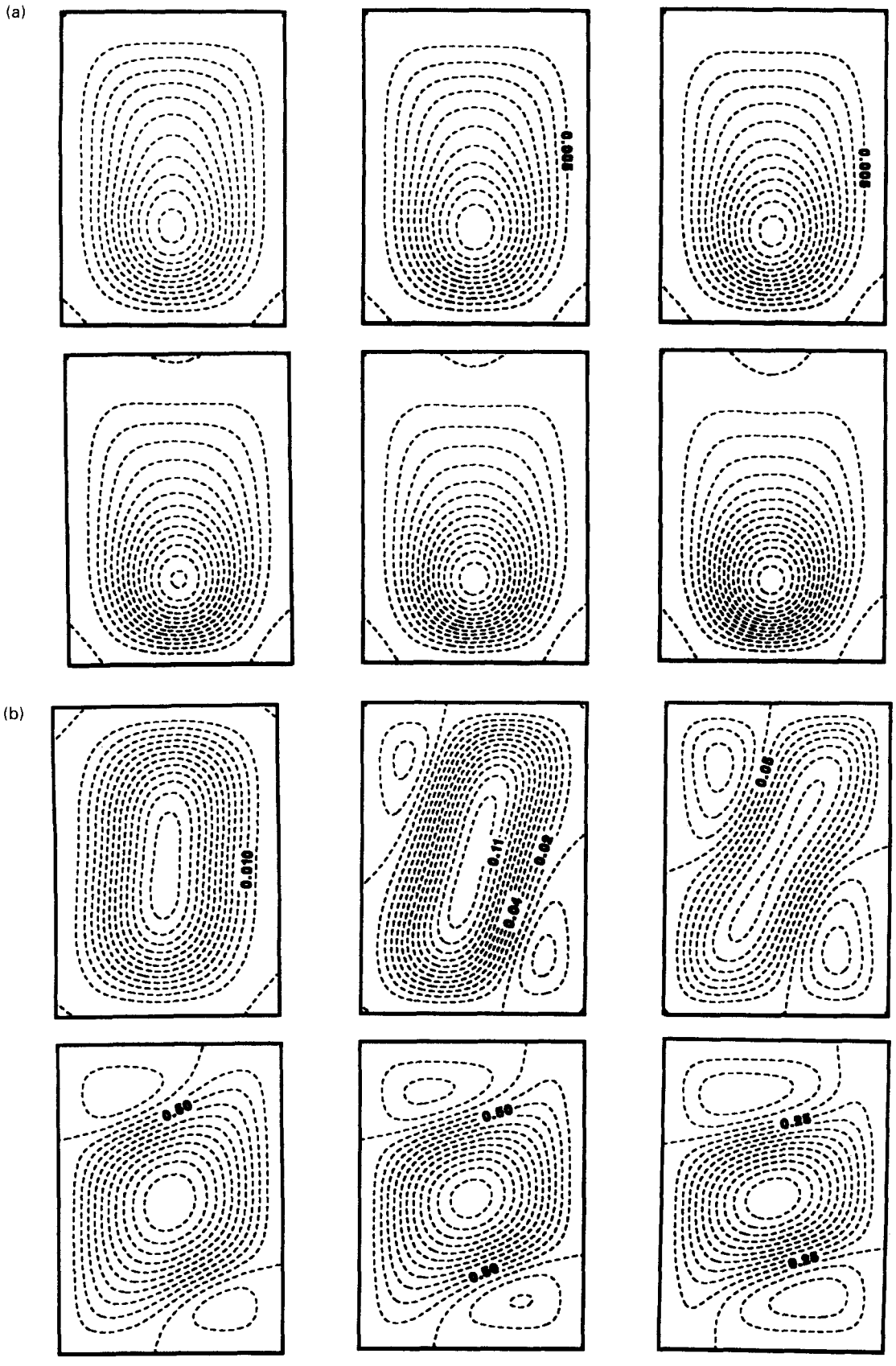

Fig. 6. Streamfunction contours for $\lambda = 0.65$ and (a) $S = 0$ Rayleigh numbers (from left to right) $R_T = 1800$, 2200, 2700, 3200, 3500 and 4000; (b) $R_T = 100$ and for density ratio numbers (from left to right) $S = 0.5$, 2.5, 6.5, 20, 25 and 30.

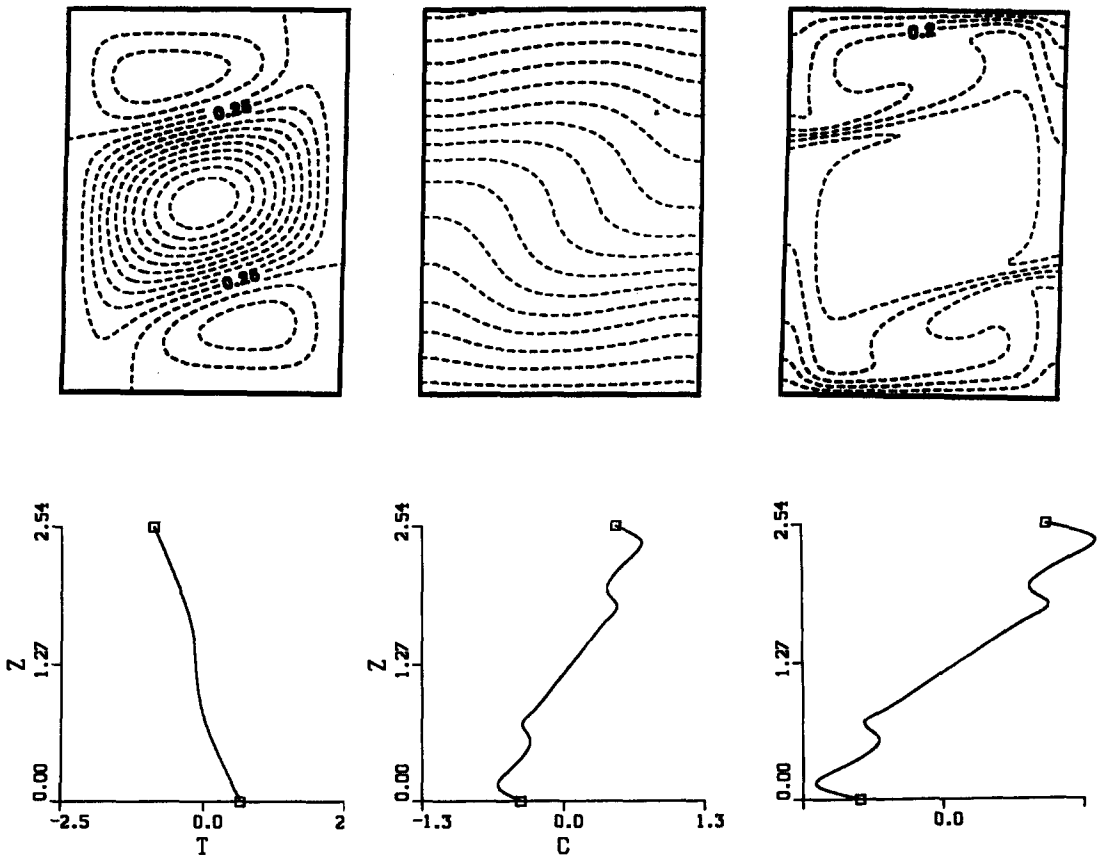

Fig. 7. Streamfunction contours, isotherms and equal concentration contours for $\lambda = 0.65$, $R_T = 100$ and $S = 30$ (top); mean profile temperature, concentration and density (bottom).

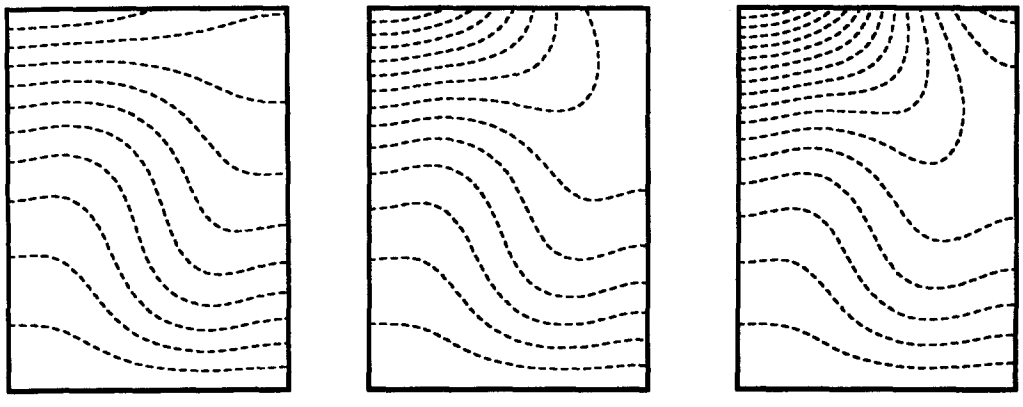

Fig. 8. Equal concentration contours for $R_T = 500$, $S = 0.05$, $\lambda = 2$ and (from left to right) $m = 10$, 30 and 50.

leigh number R_T and a density extremum parameter λ that characterize the problem of penetrative convection in pure water, two other parameters appear in this case: the density ratio S and the dimensionless liquidus slope m. Our model also incorporates the thermal effect of the layer of sea-ice [equation (12)].

The linear stability calculations successfully predict the wavenumber and instability threshold. It is demonstrated that stationary convection bifurcates from the static state in agreement with the predictions of Baines and Gill [14]. This is due to the fact that upon freezing seawater from above, a fluid parcel that is located in the upper part of the layer is both colder and saltier than one in the lower part of the layer. Consequently, both diffusing gradients act to destabilize the equilibrium profile and give rise to time-independent convection. The effects of the presence of salt, by way of the parameter S, are found to be

destabilizing. The critical wavenumbers decrease with increasing S for $\lambda < 1$, but show a very small increase with S for $\lambda = 2$. The eigensolutions of the linearized problem, equations (14) and (15), suggest that for $S = 0$ (absence of buoyancy forces due to solutal effects) and $\lambda < 1$ (the isotherm of maximum density is initially placed near the warm plate), convection sets in a layer close to the lower plate and induces weak motions in the form of a vertical stack of one or more counter-rotating vortices whose strength decreases upward. This range of parameters resembles the case of penetrative convection in pure water [5]. The generation of these weak vortices occurs primarily by way of viscous coupling at the isotherm of maximum density. Initially, this interface is located at the isotherm of maximum density. The onset of convection, however, is accompanied with the onset of the cabbeling instability which acts to move this interface upward [20].

The primary result of interest of the nonlinear calculations (system driven at up to 30 times critical) is the fact that the flow pattern consisting of one cell of intense flow near the warm plate underlying a counter-rotating cell of weak flow in the vicinity of the solid–liquid interface predominates. This is in contradistinction with the case of pure water, wherein supercritical multi-layer convection is completely inhibited. Further, we have observed the formation of concentration boundary layers near the solid–liquid interface, the warm plate and at the boundaries between the main positive cell and the negative induced cells. The centers of the vortices form cores that are both isohaline and isothermal. The mean profiles of temperature, salinity and density, displayed in Fig. 7, show that fresh and hot water rises at one edge and cold and salty water sinks at the other, with large vorticity in the center of the fluid cell. The density profile shows a double structure at the boundary layers and a uniform distribution at the center.

The nonlinear analysis seems to indicate that for supercritical Rayleigh numbers, and regardless of other parameter values, the motion is always gentle in the vicinity of the solid–liquid interface and vigorous in the lower part of the fluid cell. Therefore, within the limits of our assumptions, the results suggest that penetrative convection acts in such a way as to reduce the amount of heat that can escape to the atmosphere during the formation of a polynya.

Acknowledgements—L.H. would like to acknowledge many discussions on the coupled sea–ice–atmosphere system with A. M. J. Davis, R. McNider and W. W. Schroeder. The authors gratefully acknowledge the advice of T. Z. Mai on the numerical aspects of the problem. Fifty percent of this research was funded by the U.S. Department of Energy's (DOE) National Institute for Global Environmental Change (NIGEC) through the Southeast Regional Center at The University of Alabama-Tuscaloosa (DOE Cooperative Agreement DE–FC03–90ER61010). Financial support does not constitute an endorsement by DOE of the views expressed in this article. This work has also been supported in part by a grant from Cray Research, Inc. and with computing resources from the Alabama Supercomputer Network's Cray-C90 supercomputer.

REFERENCES

1. K. Aargaard, A. Foldvik and S. R. Hillman, The West Spitsbergen current: disposition and water mass transformation, *J. Geophys. Res.* **92,** 3778–3784 (1987).
2. A. L. Gordon and J. C. Comiso, Polynyas in the southern ocean, *Sci. Am.* **258,** 90–97 (1988).
3. S. D. Smith, R. D. Muench and C. H. Pease, Polynyas and leads: an overview of physical processes and environment, *J. Geophys. Res.* **95,** 9461–9479 (1993).
4. G. Vernonis, Penetrative convection, *Astrophys. J.* **137,** 641–663 (1963).
5. D. R. Moore and N. O. Weiss, Nonlinear penetrative convection, *J. Fluid Mech.* **61,** 553–581 (1973).
6. P. C. Mathews, A model for the onset of penetrative convection, *J. Fluid Mech.* **188,** 571–583 (1988).
7. T. D. Foster and R. Harcourt, Laboratory and numerical experiments on the cabbeling instability, *Bull. Am. Phys. Soc.* **36,** 1960 (1993).
8. J. S. Turner, Double-diffusive phenomena, *A. Rev. Fluid Mech.* **6,** 37–56 (1974).
9. R. W. Schmitt, Double diffusion in oceanography, *A. Rev. Fluid Mech.* **26,** 255–285 (1994).
10. T. D. Foster, Experiments on haline convection induced by the freezing of sea water, *J. Geophys. Res.* **74,** 6967–6974 (1969).
11. T. Farhadieh and R. S. Tankin, A study of the freezing of sea water, *J. Fluid Mech.* **71,** 293–304 (1975).
12. R. A. Brewster and B. Gebhart, The effects of supercooling and freezing on natural convection in seawater, *Int. J. Heat Mass Transfer* **37,** 543–552 (1994).
13. M. J. Molemaker and H. A. Dijkstra, Double diffusive and direct instabilities below growing sea ice, *Int. J. Heat Mass Transfer* **37,** 2547–2559 (1994).
14. P. G. Baines and A. E. Gill, On thermohaline convection with linear density gradients, *J. Fluid Mech.* **37,** 289–306 (1969).
15. B. N. Antar, Penetrative double diffusive convection, *Phys. Fluids* **30,** 322–330 (1987).
16. B. N. Antar, Penetrative double diffusive convection: effects of the Lewis number and Prandtl numbers, *Int. J. Heat Mass Transfer* **31,** 895–898 (1988).
17. A. Davey, A simple numerical method for solving Orr-Sommerfeld problems, *Q. J. Mech. Appl. Math.* **XXVI,** 402–411 (1973).
18. W. H. Press, B. P. Flannery, S. A. Teukolsky and W. T. Vetterling, *Numerical Recipes* (1st Edn), p. 251. Cambridge University Press, Cambridge (1986).
19. D. A. Anderson, J. C. Tannehill and R. H. Pletcher, *Computational Fluid Mechanics and Heat Transfer* (1st Edn), Chap. 7. Hemisphere, New York (1984).
20. T. D. Foster, An analysis of the cabbeling instability in sea water, *J.Phys. Oceanogr.* **2,** 294–301 (1972).